A nonlinear model study on the long-term behavior of shore face–connected sand ridges

D. Calvete[1] and H. E. de Swart

Institute for Marine and Atmospheric Research, Utrecht University, Utrecht, Netherlands

Received 6 August 2001; revised 19 November 2002; accepted 30 December 2002; published 31 May 2003.

[1] A morphodynamic model is analyzed to gain further knowledge about the finite amplitude behavior of shore face–connected sand ridges observed on storm-dominated inner shelves. The present work elaborates on previous studies in which it was demonstrated that ridge formation may be due to an instability of a storm-driven current moving over a sandy inner shelf with a transverse slope. Here, the long-term evolution of the ridges is studied by performing a nonlinear stability analysis in which the physical variables are expanded in eigenmodes of the linear stability problem. New physical aspects are that the longshore pressure gradient in the momentum equations and settling lag in the suspended load sediment transport are incorporated. Furthermore, along-shelf uniform shelf modes and subharmonic eigenmodes are accounted for. The model shows that after the transient stage the competition between the modes results in saturation behavior that is dominated by a few modes only. The characteristic height of the final bed forms increases with increasing transverse slopes of the shelf, while the timescale of transient behavior decreases. The longshore uniform modes, pressure gradient, and settling lag effects only have a minor effect on the dynamics. A process analysis reveals that the mechanism responsible for the saturation behavior is the sediment transport related to the bottom slope and the effect of small-scale bed forms. Subharmonic modes significantly affect the transient behavior of the ridges and cause the final bed forms to have larger amplitudes and longer wavelengths. *INDEX TERMS:* 4219 Oceanography: General: Continental shelf processes; 4255 Oceanography: General: Numerical modeling; 4558 Oceanography: Physical: Sediment transport; 3220 Mathematical Geophysics: Nonlinear dynamics; 3022 Marine Geology and Geophysics: Marine sediments—processes and transport; *KEYWORDS:* morphodynamics, nonlinear modeling, shoreface–connected ridges, saturation processes, sediment transport, inner shelf processes

Citation: Calvete, D., and H. E. de Swart, A nonlinear model study on the long-term behavior of shore face–connected sand ridges, *J. Geophys. Res.*, *108*(C5), 3169, doi:10.1029/2001JC001091, 2003.

1. Introduction

[2] Many inner continental shelves are characterized by the presence of large-scale bed forms, called shore face–connected sand ridges. Examples are the shelves along the east coast of the United States [*Swift et al.*, 1978; *Swift and Field*, 1981; *Swift et al.*, 1985], Germany [*Swift et al.*, 1978; *Antia*, 1996], Argentina [*Parker et al.*, 1982] and Holland [*van de Meene and van Rijn*, 2000]. The ridges are observed in water depths between 4 and 20 m and they extend from the offshore end of the shore face to the beginning of the outer shelf, forming an angle of 20°–35° with respect to the coastline. Their orientation appears to be related to the direction of the dominant storm-driven current: the seaward ends of the crests are shifted upstream with respect to their attachments to the shore face. Furthermore, an offshore veering of the current has been measured over the North American sand ridges. The along-shelf spacing between successive crests of shore face–connected ridges ranges between 4 and 10 km. Their height is between 1 and 6 m and they migrate in the downstream direction with velocities of (1–10) m yr^{-1}. The ridges have asymmetrical profiles, with their steepest slope on the landward sides. There is geological evidence that many shore face–connected ridges are not relict features. For example, both the ridges along the east coast of the US and on Dutch inner shelf started to form several thousands years ago and they are active under the present hydrodynamic conditions [*Swift et al.*, 1978; *van de Meene and van Rijn*, 2000; *Duane et al.*, 1972].

[3] These observations suggest that, for gaining further knowledge about the behavior of shore face–connected ridges, it is worthwhile analyzing models which describe the feedback between storm-driven currents and the sandy bottom of the inner shelf. This was first done by [*Trowbridge*, 1995]. He used depth-averaged shallow water equations for irrotational flow, supplemented with a bottom evolution equation and a simple parametrization of the

[1]Now at Department Física Aplicada, Universitat Politècnica de Catalunya, Barcelona, Spain.

0148-0227/03/2001JC001091$09.00

sediment transport (linear in the net current). He demonstrated that bed forms resembling shore face–connected ridges spontaneously form as inherent instabilities of an along-shelf uniform, storm-driven flow over a sandy microtidal inner shelf with a transverse slope. The underlying physical mechanism is the offshore deflection of the flow over the shoals and the related loss of sediment carrying capacity in the offshore direction. The latter is due to the transverse bottom slope. In subsequent studies the model of [*Trowbridge*, 1995] was extended with additional physical effects. [*Falqués et al.*, 1998a, 1998b] included bottom friction and Coriolis forces in the momentum equations and they also modified the sediment transport by including the tendency of the sediment to move downhill. As a result they were able to demonstrate the presence of preferred bottom modes which initially have the largest growth rates. [*Calvete et al.*, 2001b] showed that tidal currents only have a small effect on the growth of shore face–connected ridges. [*Calvete et al.*, 2001a] incorporated suspended load sediment transport and depth-dependent stirring of sediment by waves in the model. They showed that these aspects are important for obtaining realistic spatial patterns, migration speeds and *e*-folding timescales of growth.

[4] A major limitation of the models listed above is that perturbations are assumed to have very small amplitudes, hence they only describe the initial formation of the ridges. In order to study their long-term evolution the model has to account for nonlinear effects like mode competition. This problem was studied by [*Calvete et al.*, 1999, 2002], where in the latter study significant improvements in the physical model formulation were made. Their method involves a spectral expansion of the physical variables (like velocity, bottom level) in a truncated series of linear eigenmodes. In this way the method provides for a natural extension of the linear analysis. It was found that nonlinear dynamics results in saturation behavior of shore face–connected ridges; that is, after a transient stage the height of the bed forms becomes constant. The final height is roughly linearly correlated with the slope of the inner shelf, while the timescale of the transients decreases. However, in none of these studies was the physics causing the saturation behavior discussed.

[5] The first objective of the present paper is therefore to analyze the physical processes that are responsible for the saturation behavior of shore face–connected sand ridges. The second is to study the influence on the amplitude behavior of new physical processes in the morphodynamic model. These include the forcing of the storm-driven current by a longshore pressure gradient and the finite settling time of the suspended sediment particles. These new processes affect the cross-shelf profile of the storm-driven current and the erosion/deposition of sediment, respectively, and thereby the properties of the ridges. The third objective is to investigate the role of new types of modes in the spectral expansions. One of them is the so-called $k = 0$ mode, which has an along-shelf uniform structure. This mode is generated by self-interaction of the wave-like perturbations. Examples of $k = 0$ phenomena are wave-induced setup/setdown of water levels in the nearshore zone and net currents driven by radiation stresses and/or tidal stresses. The relevance of the $k = 0$ mode for long-term morphodynamics has been shown by [*Komarova and Newell*, 2000]. The other new modes that are investigated are subharmonic modes, having wavelengths that are longer than that of the preferred mode. They are included by considering an along-shelf domain length that is a multiple of the preferred wavelength. Their incorporation in the spectral expansions results in new and potentially important nonlinear interactions.

[6] The nonlinear stability method applied in this paper requires the formulation of a morphodynamic model, the determination of a basic state and knowledge about the characteristics of the eigenmodes that can initially develop as free instabilities on this basic state. These aspects are all discussed in the next section, including an outline of the subsequent nonlinear solution method. The model is restricted to microtidal storm-driven inner shelves like the shelf of Long Island (east US coast), described in section 3. Model results are discussed in section 4. The final section contains a discussion and concluding remarks.

2. Model

[7] In subsections 2.12.2 to 2.3, we give an outline of the model equations, which are used to describe the long-term evolution of shore face–connected ridges on storm-dominated inner shelves [for details see *Calvete et al.*, 2001a]. Since these ridges merely evolve during stormy weather, we assume that our model equations are representative for the situation during storms. In subsection 2.4 the basic state and the linear stability analysis is discussed. The nonlinear solution method is outlined in subsection 2.5.

2.1. Equations of Motion

[8] The hydrodynamics is modelled by the depth- and wave-averaged shallow water equations:

$$\frac{\partial \vec{v}}{\partial t} + \left(\vec{v}\cdot\vec{\nabla}\right)\vec{v} + f\vec{e}_z \times \vec{v} = -g\vec{\nabla}z_s + \frac{\vec{\tau}_s - \vec{\tau}_b}{\rho D}\,, \tag{1a}$$

$$\frac{\partial D}{\partial t} + \vec{\nabla}\cdot(D\vec{v}) = 0\,. \tag{1b}$$

[9] Here $\vec{v}$ is the velocity vector, D the total depth of the fluid and z_s the elevation of the free surface with respect to its undisturbed level. Furthermore, $f(\sim 10^{-4}\ \mathrm{s}^{-1})$ is the Coriolis parameter, $g(\sim 10\ \mathrm{m\ s}^{-2})$ the acceleration due to gravity, $\rho(\sim 10^{3}\ \mathrm{kg\ m}^{-3})$ the density of the water, $\vec{\tau}_s$ the wind stress at the surface and $\vec{\tau}_b$ the bed shear stress. Finally t is time and $\vec{\nabla}$ the horizontal nabla operator.

[10] The location of the bottom with respect to the still water level is denoted by z_b. Conservation of total sediment mass yields the bottom evolution equation

$$(1-p)\frac{\partial z_b}{\partial t} + \vec{\nabla}\cdot\vec{q} = 0\,. \tag{2}$$

Here $p(\sim 0.4)$ is the bed porosity and $\vec{q}$ the volumetric sediment flux (excluding the pores) per unit width. The parameterizations of the bed shear stress vector $\vec{\tau}_b$ and the sediment flux $\vec{q}$ are discussed in the next subsection.

[11] These equations of motion are solved in a domain as shown in Figure 1. It represents an idealized inner shelf that

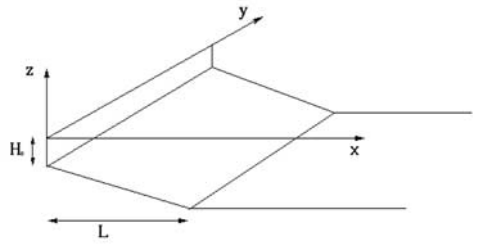

Figure 1. Sketch of the geometry and the coordinate system. For explanation of the symbols see the text.

is bounded on its shallow side (at $x = 0$) by the shore face and on its deep side (at $x = L$) by the outer shelf. A Cartesian coordinate system is used with x, y, and z axis pointing in the cross-shelf, along-shelf, and vertical direction, respectively. The x and y components of the velocity vector $\vec{v}$ are denoted by u and v, respectively.

[12] The boundary conditions are that the cross-shelf velocity component u vanishes at the boundaries $x = 0$ and $x \to \infty$. Moreover, the undisturbed water depths $H(x = 0)$ and $H(x > L)$ are kept fixed at their values H_0 and H_L, respectively. In the along-shelf direction periodic boundary conditions will be used where the basic length, L_y, will be fixed later on.

2.2. Bed Shear Stress and Sediment Transport During Storms

[13] During storms the water motion on the inner shelf is characterized by large wave orbital motion with respect to the magnitude of the depth- and wave-averaged currents. This allows for a linearization of the quadratic bottom friction law, yielding the bed shear stress formulation

$$\vec{\tau}_b = \rho r_* \vec{v} .$$

Here r_* is a friction coefficient which is proportional to the drag parameter c_d and the velocity amplitude u_w of the wave orbital motion. We will assume that the latter quantity depends on the local water depth as follows:

$$u_w^2 = u_{w0}^2 \left(\frac{\langle z_b \rangle}{H_0} \right)^{-m}, \qquad r_* = r_{*0} \left(\frac{\langle z_b \rangle}{H_0} \right)^{-m/2} .$$

The brackets $\langle . \rangle$ indicate an average in the along-shelf (y) direction and the subscript 0 indicates the value of a variable at $x = 0$. In this model the intensity of the wave orbital motion decays algebraically with increasing values of the along-shelf-averaged water depth $\langle z_b \rangle$ with an exponent m. Typical values are $u_{w0} \sim 1$ m s^{-1}, $r_{*0} \sim 10^{-3}$ m s^{-1} and $m \sim 1.6$.

[14] The volumetric sediment flux per unit width during storms reads

$$\vec{q} = \vec{q}_b + \vec{q}_s ,$$

where $\vec{q}_b$ and $\vec{q}_s$ denote the bed load and suspended load part. Expressions for the latter are derived from the formulations originally introduced by [*Bailard*, 1981], but modified such they apply to depth-averaged flow during storms and account for settling lag effects and depth-dependent deposition in the suspended load transport. For the bed load flux this yields

$$\vec{q}_b = \nu_b \left[u_w^2 \vec{v} - \lambda_b u_w^3 \vec{\nabla} h \right] ,$$

where $\nu_b \sim 4 \times 10^{-5}$ s^2 m^{-1}, $\lambda_b \sim 0.4$ and h the bottom perturbation with respect to the undisturbed level $z = -H(x)$. The first contribution describes the stirring of sediment by waves and the subsequent transport by the net current. The quantity $\nu_b u_w^2$ is the wave stirring coefficient. The second accounts for the tendency of the sediment to move downslope. Note that the downslope component of the sediment transport due to the reference bathymetry $z = -H(x)$ is not modelled. It is assumed that the equilibrium profile is maintained by processes (such as wave asymmetry) which are not explicitly considered in the present model.

[15] The suspended load flux is modelled as

$$\vec{q}_s = \vec{v} \mathcal{C} - \lambda_s u_w^5 \vec{\nabla} h ,$$

where $\mathcal{C}$ is the depth-averaged relative concentration of suspended sediment. The latter obeys the equation

$$\frac{\partial \mathcal{C}}{\partial t} + \vec{\nabla} \cdot (\vec{v} \mathcal{C}) = w_s (c_a - c_b) , \tag{3}$$

with w_s the settling velocity of the sediment particles, c_a the reference concentration and c_b the concentration at the top of the active layer. Here c_a is parameterized according to [*van Rijn*, 1993] and a relation between c_b and C is obtained from the equilibrium sediment concentration profile by using a depth-dependent turbulent vertical diffusion coefficient. This yields

$$c_a = \left(\frac{u_w}{\hat{u}} \right)^3 , \qquad c_b = \frac{\mathcal{C}}{\delta H} , \qquad \delta^{-1} = (\delta_0)^{-1} \left(1 + \frac{h}{H} \right) .$$

Here $\hat{u}$ is a velocity proportional to the depth-averaged critical velocity of erosion, δH is the thickness of the suspended load sediment layer and $\delta_0 H$ is its along-shelf averaged value. Typical values are $w_s \sim 0.05$ m s^{-1}, $\hat{u} \sim 10$ m s^{-1}, $\delta_0 \sim 0.15$ and $\lambda_s u_{w0}^5 \sim 1 \times 10^{-4}$ m^2 s^{-1}.

2.3. Approximations

[16] In [*Calvete et al.*, 2001a] the equations of motion were made nondimensional by using appropriate scales of motion, resulting in several simplifications. The first is the so-called quasi-steady approximation: time derivatives are neglected in all equations, except in the bed evolution equation. The reason is that the bottom changes take place on a much longer timescale (order of decades) than that of the fluid (order of days). Thus, if the focus is on morphodynamic developments, it can be assumed that the fluid instantaneously adjusts to changes in the bottom profile. The second simplification is the rigid lid approximation: variations of the free surface are neglected, except in the pressure gradient terms in the momentum equations. This is implied by the fact that the typical amplitude of the sea surface elevations is much smaller than the undisturbed

water depth, hence the Froude number of the flow is very small.

2.4. Basic State and Linear Stability Analysis

[17] The model allows for a basic state which has a uniform structure in the along-shelf direction. It is characterized by

$$\vec{v} = (0, V(x)), \quad z_s = s_* y + \xi(x),$$

$$\mathcal{C} = C(x), \qquad z_b = -H(x).$$

Substituting these expressions in equations (1a) and (3), and using the assumptions listed in section 2.3, it follows that

$$f V = g \frac{\mathrm{d}\xi}{\mathrm{d}x}, \qquad 0 = -g s_* + \frac{(\tau_{sy} - \tau_{by})}{\rho H},$$

$$\left(\frac{u_w}{\hat{u}}\right)^3 - \frac{C}{\delta H} = 0.$$

The first equation given above describes the cross-shelf setup (or setdown) of the mean water level due to a cross-shelf water level gradient and Coriolis effects. The second equation is the along-shelf momentum balance due to the water level gradient s_*, the wind stress component τ_{sy} and bottom friction, which determines the along-shelf current profile $V(x)$. The final equation shows a balance between the pickup and deposition of sediment near the bed. Substitution of the relations given above in equation (1b) shows that mass conservation is verified identically. Since this basic state obeys the bottom evolution equation (2) for a fixed bed level, it represents a morphodynamic equilibrium.

[18] Next, we consider the dynamics of small perturbations evolving on this basic state. This is done by defining

$$\Phi = (\vec{v}, \eta, \mathcal{C}, z_b)$$

as the solution vector of our model equations (1a), (1b), (2), and (3). Now consider solutions of the form

$$\Phi = \Phi_b + \phi,$$

where $\Phi_b = (0, V(x), s_* y + \xi(x), C(x), -H(x))$ denotes the basic state and $\phi = (u, v, \eta, c, h)$ the perturbations. Substitution of these solutions in the equations of motion yields the results as shown in appendix A. These equations can be symbolically written as

$$S \frac{\partial \phi}{\partial t} = \mathcal{L}\phi + \mathcal{N}(\phi), \tag{4}$$

where S is a matrix and $\mathcal{L}$ a linear operator involving spatial derivatives. Finally $\mathcal{N}$ includes all nonlinear terms in the equations of motion for the perturbations.

[19] The linear system, i.e $\mathcal{N}(\phi) = 0$ in equation (4), allows for wave-like solutions which travel in the y direction: $\phi(x, y, t) = \mathrm{Re}\,(\tilde{\phi}(x) e^{iky + \omega t})$, where Re denotes the real part. Here k is a wave number in the alongshore direction with $\lambda = 2\pi/k$ the corresponding wavelength. Furthermore, ω is a complex frequency, which can be written as $\omega = \sigma - \mathrm{i}kv_{mi}$, with σ the growth rate and v_{mi} the migration speed in the y direction. Exponentially growing solutions have a positive growth rate, i.e., $\sigma > 0$, with an e-folding time $\tau = \sigma^{-1}$.

[20] The complex frequency, ω, and the cross-shelf structure of the perturbations, $\tilde{\phi}$, follow as solutions of the eigenvalue problem

$$\omega S \tilde{\phi} = \mathcal{L}_k \tilde{\phi}. \tag{5}$$

Operator $\mathcal{L}_k$ is obtained from operator $\mathcal{L}$ in equation (4) by replacing derivatives $\partial/\partial y$ by ik. Solutions of the eigenvalue problem equation (5) depend on the model parameters (the transverse slope β of the shelf, forcing conditions, storm fraction, bottom friction parameter, Coriolis parameter, settling time, wave orbital motion). They are obtained numerically by applying a collocation method.

2.5. Nonlinear Analysis: Derivation of Amplitude Equations

[21] To model the long-term behavior of the perturbations, we return to the full equations of motion (4). Approximate solutions of such a system can be obtained by applying spectral methods [cf. *Canuto et al.*, 1988]. This means that the solutions are expanded in a suitable set of spatial modes. In the present study we will use eigenmodes of the linear problem as the expansion modes and perform a Galerkin procedure to derive the amplitude equations. This is done by first writing the perturbations as

$$\phi(x, y, t) = \langle \phi \rangle(x, t) + \phi'(x, y, t) \tag{6}$$

where $\langle \phi \rangle$ are the contributions having an along-shelf uniform structure. The contributions $\phi'(x, y, t)$ are expanded in eigenmodes of the linear problem with specific nonzero along-shelf wave numbers k_j:

$$\phi'(x, y, t) = \sum_j \sum_{n_j} \begin{pmatrix} \hat{u}(t)\tilde{u}(x) \\ \hat{v}(t)\tilde{v}(x) \\ \hat{\eta}(t)\tilde{\eta}(x) \\ \hat{c}(t)\tilde{c}(x) \\ \hat{h}(t)\tilde{h}(x) \end{pmatrix}_{j n_j} e^{ik_j y} + \text{c.c.} \tag{7}$$

An individual mode is denoted by (j, n_j), where j and n_j refer to the along-shelf, Fourier, mode k_j and cross-shelf mode number, respectively. Increasing cross-shelf mode numbers imply decreasing growth rates. Furthermore $\tilde{u}$, $\tilde{v}$, etc. denote the known cross-shelf structures of the eigenfunctions. The unknowns are the functions $\langle \phi \rangle(x, t)$ and the amplitudes $\hat{u}$, $\hat{v}$, $\hat{\eta}$, $\hat{c}$, $\hat{h}$, for all the (j, n_j) modes.

[22] Second, the expansions (6)–(7) are substituted in the nonlinear equations of motion (4) (see appendix A). Next, the equations are averaged over the along-shelf y direction. This yields a differential equation for the longshore uniform bottom mode $\langle h \rangle(x, t)$ and four algebraic equations for the longshore uniform flow modes $\langle u \rangle$, $\langle v \rangle$, $\langle \eta \rangle$ and $\langle c \rangle$, see appendix B. Finally, the equations for the $k = 0$ mode are substracted from the original equations and the results are projected onto the adjoint eigenfunctions of the linear problem. The result of this Galerkin projection is a system

of nonlinear differential equations for the amplitudes of the bottom modes $\hat{h}_{j,nj}$ and algebraic equations for the corresponding amplitudes $\hat{u}_{j,nj}$, $\hat{v}_{j,nj}$, $\hat{\eta}_{j,nj}$ and $\hat{c}_{j,nj}$. In a symbolic form they read

$$0 = L_1 U + M_1 h + f(U, h, \langle\phi\rangle) \tag{8a}$$

$$\frac{\mathrm{dh}}{\mathrm{dt}} = L_2 U + M_2 h + g(U, h, \langle\phi\rangle) \tag{8b}$$

where L_1, L_2, M_1 and M_2 are matrices, h is a vector including all bottom amplitudes and U is a vector with all other amplitudes.

[23] A finite dimensional system is obtained when a finite number of eigenmodes is included in the expansion (7). This is done by considering solutions in a domain with length L_y in the along-shelf direction and with periodic boundary conditions. Consequently, only specific values of the along-shelf wave numbers are allowed for. If we assume that a total number J of different longshore wave numbers k_j ($=2\pi j/L_y$) is included and N_J is the maximum cross-shelf mode number, then system of equations (8a) and (8b) contains $5 \times J \times N_J$ equations. The resulting system is solved by using a third-order time integration scheme [see *Karniadakis et al.*, 1991]. The numerical model that solves this problem is called MORFO45. The solutions are assumed to give an accurate description of the solution of the original model if their characteristics do not change with further increase of the truncation numbers J and N_J.

3. An Example Case: Long Island Inner Shelf

[24] The Long Island inner shelf is located at 40° latitude on the Northern Hemisphere. This is a prototype storm-dominated inner shelf on which a clearly recognizable patch of shore face–connected ridges is observed [cf. *Swift et al.*, 1985]. Its depth varies from $H_0 = 14$ m at the shore face side to $H_L = 20$ m on the seaward side over a distance $L = 5.5$ km. Field data indicate that the along-shelf-averaged water depth almost linearly increases with increasing distance from the coast. Hence the bottom profile can be described by

$$H(x) = \begin{cases} H_0 + \beta x & (0 \le x \le L) \\ H_L & (x > L) \end{cases}$$

where the slope is $\beta \sim 1 \times 10^{-3}$. The sediment in this area has a mean grain size of about 4×10^{-4} m. The shore face–connected sand ridges on this shelf have an along-shelf spacing of about 3.5 km, their height is ~4 m and they migrate southward with a typical velocity of (2–3) m yr^{-1}. [*Duane et al.*, 1972] state that the age of these ridges is younger than 11000 yr and the time that they needed to develop was of the order of 1000 yr.

[25] At this location storms typically occur about 5% of the total time and are characterized by waves coming from the north east, a southward directed wind stress of about 0.4 N m^{-2} and a small longshore pressure gradient of about $s_* = 2 \times 10^{-7}$. This induces both a strong wave orbital motion (characteristic velocity amplitude at the shore face of about $u_{w0} = 1$ m s^{-1}) and a southward net flow with a typical velocity of 0.4 m s^{-1} that increases in the offshore direction [see *Niedoroda and Swift*, 1981; *Niedoroda et al.*, 1984]. Moderate tidal currents, of the order of 0.2 m s^{-1}, were reported by [*Scott and Csanady*, 1976] from a moored buoy at 11 km from the shore of Long Island. The tidal range is 0.7–1.0 m. The bottom friction coefficient is $r_{*0} = 1 \times 10^{-3}$ m s^{-1}. An exponent $m = 1.6$ is used in the expression of the wave orbital motion (see section 2.2) and $\delta_0 = 0.15$ is taken for the relative thickness of the suspended load layer. The characteristic magnitudes of suspended load transport and bed load transport then read $Q_S \sim 8 \times 10^{-4}$ m^2 s^{-1} and $Q_B \sim 2 \times 10^{-5}$ m^2 s^{-1}, respectively.

4. Results

[26] Runs were performed with the nonlinear model for parameter values representative for the Long Island shelf. The default experiment includes the $k = 0$ mode, the effect of a finite settling time in the concentration equation and the longshore pressure gradient. The longest wavelength included in the eigenfunction expansion is that of the initially fastest growing mode.

[27] In section 4.1 we present the results of the linear analysis, which are necessary for the subsequent study of the long-term evolution of the ridges. In section 4.2 the effect of new physical processes and the $k = 0$ mode on the model behavior is studied. This is done by exploring the dependence of the solutions on the transverse slope β. The results are then compared with the ones obtained by [*Calvete et al.*, 2002]. As will be explained below, this procedure is necessary to predict the model behavior for a measured value of the transverse slope. The information is also used in section 4.3 to select a specific value of β, for which the saturation behavior of the ridges is analyzed. Finally, in section 4.4 the influence of adding subharmonic modes in the spectral expansions is investigated.

4.1. Basic State and Linear Stability Analysis

[28] The profiles of $V(x)$ and the concentration $C(x)$ of the basic state for the bathymetry $H(x)$ of the Long Island inner shelf are shown in Figure 2. The growth rate and migration speed of the linear perturbations for different cross-shelf mode numbers are shown in Figure 3 as functions of the along-shelf wave number k. The fastest growing mode (also called the most preferred mode) has a wave number $k \sim 1.5$ km^{-1} ($\lambda = 4.1$ km) and a growth rate $\sigma \sim 8 \times 10^{-3}$ yr^{-1} ($\tau \sim 125$ yr). This mode migrates ~2 m yr^{-1} in the downstream direction and has an up-current orientation (Figure 4), consistent with field observations of shore face–connected ridges (section 3).

[29] In Figure 5 the e-folding timescale τ, longshore spacing λ and migration speed v_{mi} of the most preferred mode are shown as functions of the transverse slope β. Ridges only grow for slopes larger than the critical value β_c. For parameter values representative for the Long Island shelf, $\beta_c \sim 0.5 \times 10^{-4}$, $\lambda_c = 11$ km and $v_{mic} = -2.6$ m yr^{-1}. Both the growth rate, spacing and migration speed decrease with increasing values of the transverse slope.

4.2. Role of New Physical Processes and of the $k = 0$ Mode

[30] In this study the values of the spectral parameters are $J = 20$, $N_J = 16$, and 100 collocation points. A time step of

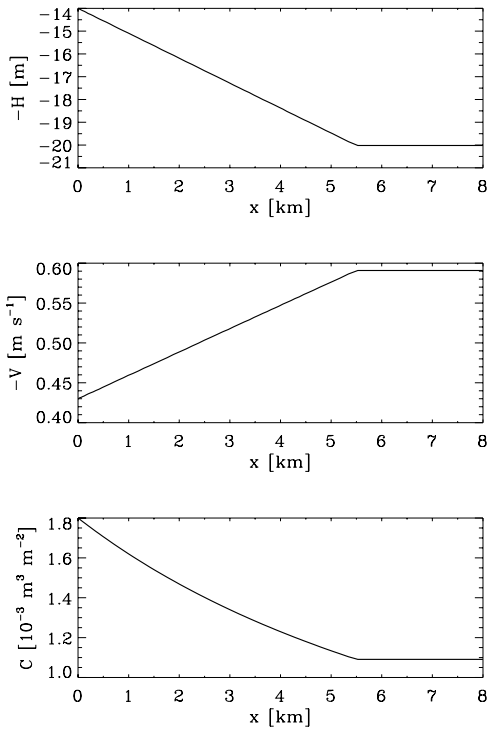

Figure 2. Basic state (top) bathymetry, (middle) alongshelf velocity profile, and (bottom) concentration profile for the default inner shelf (Long Island).

$\Delta t = 0.4$ yr resulted in computational stability in all the runs discussed here.

[31] Experiments revealed that, if the measured transverse slope was taken as a value for parameter β, the run could not be fully analyzed. Simulations performed with smaller values of β did not encounter this limitation. These results motivated the application of a procedure in which β was increased with small steps and the dependence of the model properties on this parameter was systematically explored. These findings could then be extrapolated to predict the model behavior for large values of β (section 5).

[32] It was found that, consistent with the linear analysis, perturbations only grow if β is larger than its critical value β_c. In that case their amplitudes reach saturation values after a finite period of time, i.e., the saturation time. Thus the model describes the tendency to form migrating shore face–connected ridges with finite and constant amplitudes. In Figure 6 the amplitude of the final bottom perturbations and the saturation time are shown as functions of β. For large values of the transverse slope ($\beta > 5.0 \times 10^{-4}$), solutions become unbounded some time before the saturation is reached.

[33] Figure 6 indicates an almost linear relation between the final amplitude and β. The amplitude of the perturbation is ~65% of the depth difference between the depth at the end of the shore face and the depth at the transition to the outer shelf. The saturation time decreases with increasing values of the transverse slope. The time needed to reach an equilibrium is approximately 6 times the *e*-folding timescale of the initially most preferred mode. For $\beta = 5.0 \times 10^{-4}$ the saturation time is ~2000 yr with an amplitude of the ridges of ~1.7 m.

[34] The spatial pattern of the bottom perturbation and that of the total depth are shown in Figure 7 for $\beta = 1.0 \times 10^{-4}$, 2.5×10^{-4} and 5.0×10^{-4}. The profiles in the alongshelf direction are asymmetrical with steeper slopes on the downstream sides. This degree of asymmetry increases with increasing β. For large values of the transverse slope also

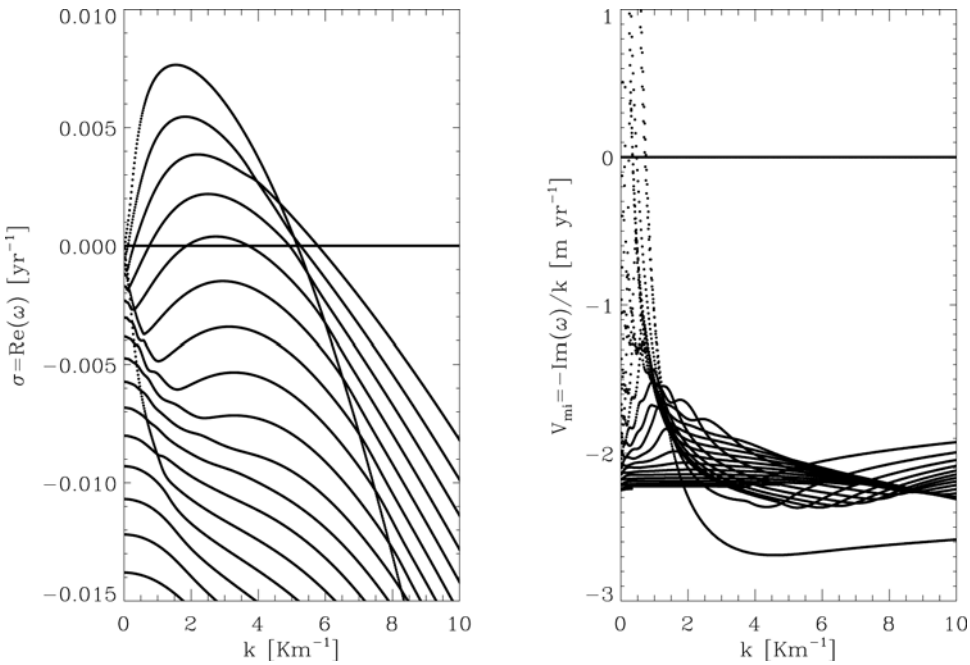

Figure 3. (left) Growth rate and (right) migration speed of small perturbations evolving on the basic state as a function of the along-shelf wave number *k*. Different curves represent different cross-shelf mode numbers. Parameter values are representative for the Long Island inner shelf.

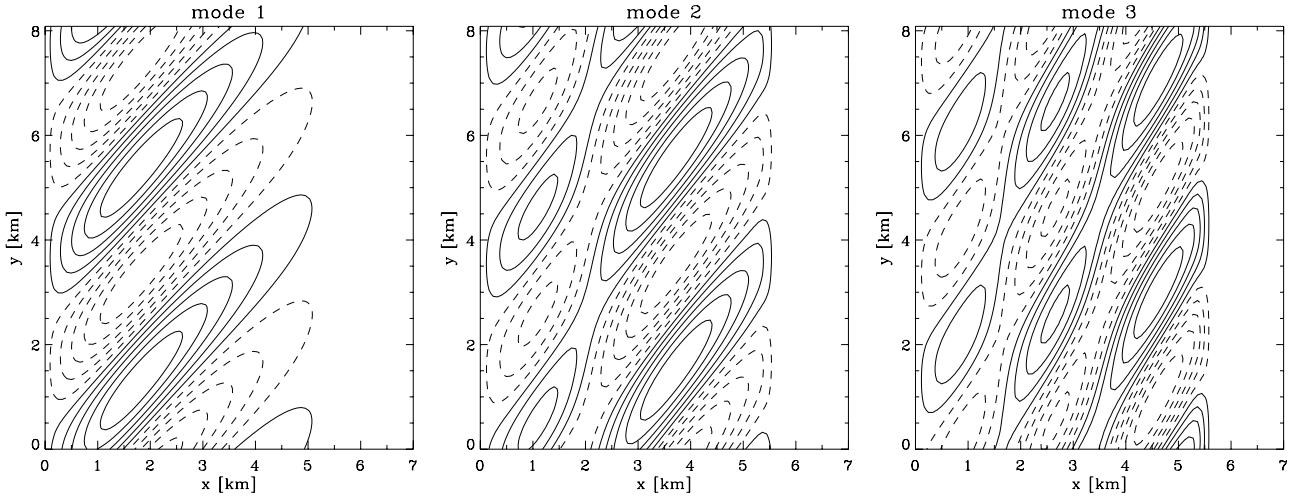

Figure 4. First three bottom modes (different cross-shelf mode numbers) in case of the default shelf and along-shelf wave number $k = 1.5$ km^{-1}. Mode 1 has the largest growth rate; the current is directed from top to bottom. For illustrative reasons, two ridges are shown.

relatively small-scale bed forms, with wavelengths in the order of a few hundred meters, are present. The migration speed of the saturated bed forms is almost identical to the one of the initially fastest growing mode.

[35] Comparison of these results with those obtained by [*Calvete et al.*, 2002] reveals that adding an along-shelf pressure gradient and taking account of finite settling times of suspended sediment particles do not have a large effect on the finite amplitude behavior of the ridges. A large number of experiments were carried out in which the magnitude of the along-shelf pressure gradient was varied (hence the profile of the current $V(x)$ was changed) and all other parameter values were fixed. It was found that these changes have only a small influence on the final results. Besides, runs were performed in which the settling time of the sediment was varied. Again, results were almost identical to those shown in this section.

[36] The $k = 0$ mode does not play an important role in the dynamics since its amplitude is only about 5% of that of the nonuniform perturbations ($k \neq 0$). Physically this means that there is hardly any exchange of sediment between inner shelf and shore face. The along-shelf-averaged profile becomes slightly deeper near the shore face and slightly shallower on the seaward side.

4.3. Physics of the Saturation Processs

[37] The saturation behavior of the model is investigated for a fixed value ($\beta = 2.5 \times 10^{-4}$) of the transverse slope. This relatively small value for β will yield a clear insight into the mechanisms at work. The time evolution of the amplitudes of the bottom modes and of the height of the perturbation are shown in Figure 8. A similar analysis has been made for a more realistic value of the transverse slope, i.e., $\beta = 5.0 \times 10^{-4}$, resulting in identical conclusions. The analysis in this case is more complicated, because the prominent presence of small-scale bottom features causes significant small-scale erosion-deposition patterns. The solutions are analyzed at $t = 2400$ yr, when the ridges are still growing, and at $t = 4800$ yr, when the ridges have reached their final height and are only migrating. The total depth and

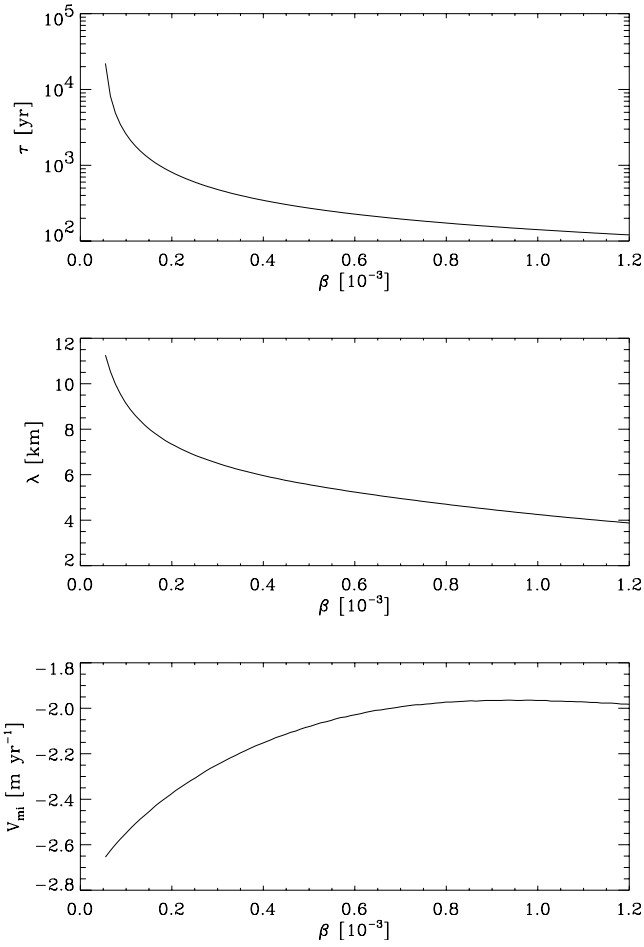

Figure 5. The *e*-folding timescale, along-shelf wavelength, and migration speed of the initially most preferred mode as a function of the transverse slope β. Other parameter values representative for the Long Island shelf.

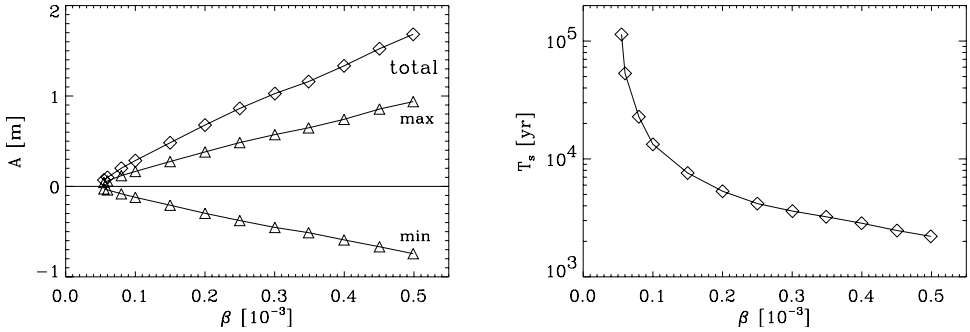

Figure 6. Amplitude of the bed forms at the (left) final state and (right) saturation time as a function of the transverse slope β. Parameter values representative for the Long Island shelf.

perturbation of the bottom at these two times are shown in Figure 9. The dashed lines indicate sections along which profiles of the physical variables will be made.

[38] The bottom pattern at t = 2400 yr resembles that of the initially most preferred mode. The total depth is characterized by a smooth along-shelf pattern. At t = 4800 yr the bottom has a more asymmetrical profile and small-scale perturbations are superimposed on the large-scale ridges. An inspection of the cross-shelf and along-shelf profiles of the velocity, the concentration and the bottom at t = 2400 yr along two sections shows that there is an almost linear relationship between the perturbed hydrodynamic variables and the perturbed bottom. The along-shelf and cross-shelf velocity increase above the ridges whereas the depth-integrated concentration becomes smaller above the crests. At t = 4800 yr, see profiles in Figure 10, similar relations are observed.

[39] The subplots in Figure 10 indicate that the current has an offshore deflection over the ridges. This deflection is responsible for the initial ridge growth, as was already

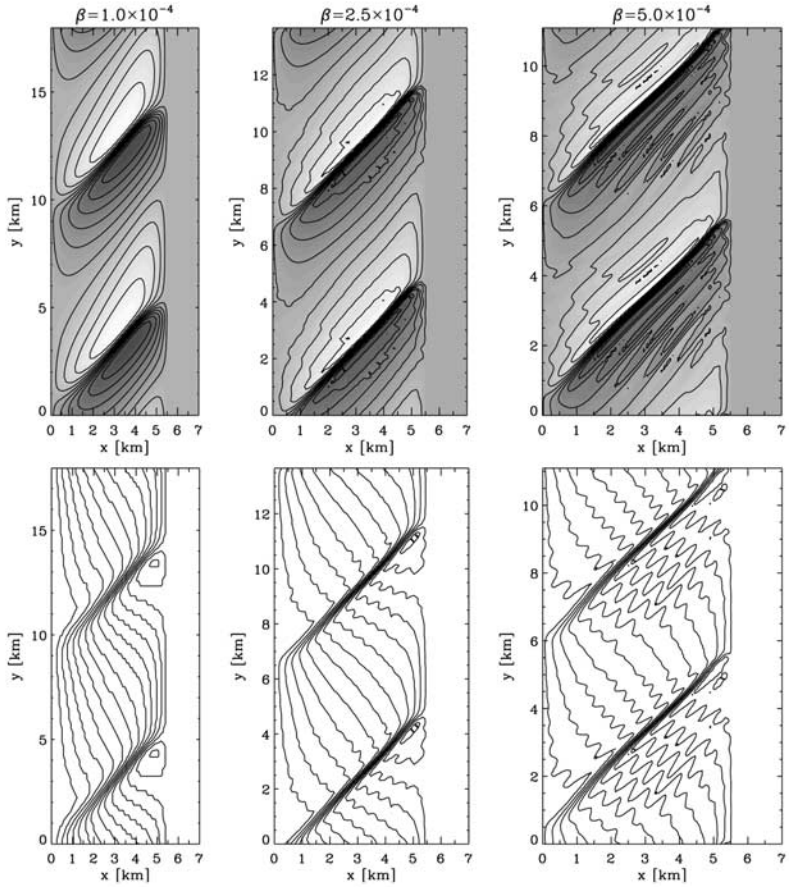

Figure 7. Contour plots of the (top) bottom perturbation and (bottom) total depth after saturation for different values of β. The current is directed from top to bottom.

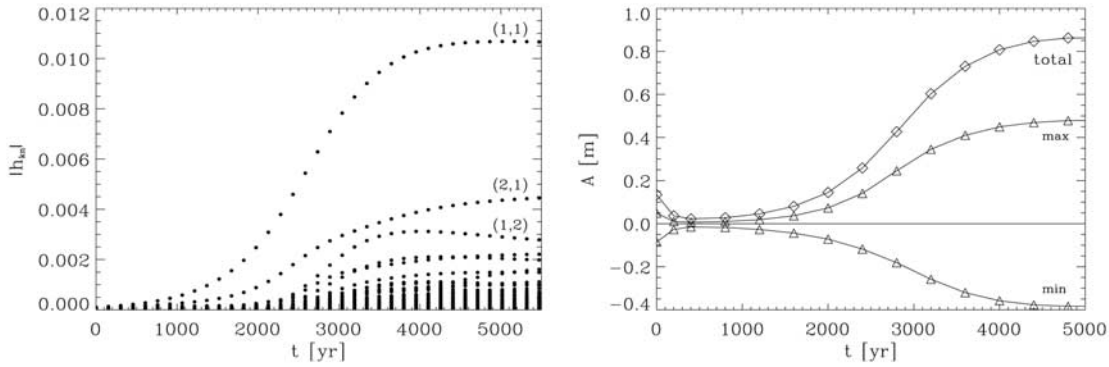

Figure 8. (left) Time evolution of the amplitude of the different bottom modes for $\beta = 2.5 \times 10^{-4}$. (right) As the left subplot, but for the maximum and minimum elevation, as well as for the total height of the bottom perturbation.

pointed out by [*Trowbridge*, 1995]. It is remarkable that the positive feedback between the current and bottom is still present at the saturated state. Clearly, the saturation behavior of the ridges is not related to a change in the hydrodynamic conditions due for example to a frictional effect or bar reorientation.

[40] Insight into the saturation process is obtained by determining the various contributions to the divergence of the total sediment transport (erosion-deposition) and comparing their profiles with that of the corresponding bottom perturbation. In Figures 11 and 12 such profiles are shown along the two sections indicated in Figure 9. The divergence of the sediment flux is split into different terms: advection of suspended load (subplots a and g), advection of bed load (b, h) and diffusive terms (c, i). The divergence of the total sediment transport (d, j) is the superposition of the various contributions. Finally, in subplots (e) and (k) the profiles of erosion-deposition related to the advective terms (solid line) and the diffusive ones (dashed line) are plotted.

[41] At $t = 2400$ yr, the suspended load terms produce a deposition over the highest part of the ridge and erosion in the lower part. Maximum deposition and erosion take place at the leeward sides and this forces the slope to become steeper. The overall effect of this term is a further increase of the amplitude and a more asymmetrical ridge. The deposition related to the advective part of the bed load takes place only at the leeward sides and small erosion occurs at the stoss sides. This term is responsible for the migration of the ridges. Diffusive terms related to both suspended and bed load processes on the other hand tend to reduce both the along-shelf asymmetry of the ridge and its amplitude. At this stage of the ridge growth, diffusive terms are already quite large, when compared with their values at the initial growth stage. The net pattern of erosion-deposition of the total sediment transport at this stage will cause the ridge to become higher and steeper, while it keeps on migrating.

[42] At $t = 4800$ yr (Figure 12) the general behavior of the different terms is similar, with the exception of two new phenomena that are important for the saturation. One is that there are now small-scale oscillations superimposed on the global trend; the other is that the magnitude of the diffusive contributions is similar to that of advective terms. The small-scale features are generated by nonlinear processes. The latter originate from the advective terms in the suspended load transport, since the other terms are linear. In Figure 13 the total and linear contribution to the divergence of the advective part of the suspended load flux are plotted. Apart from enhancing small-scale features, the nonlinear terms cause a shift in the erosion-deposition pattern toward the leeward sides of the ridges. Because of the larger asymmetry, the diffusive contributions in the sediment transport increase and compensate the advective contributions.

4.4. Effect of Subharmonic Modes

[43] So far we have presented results for the resolved modes consisting of the initially most preferred mode (with along-shelf wavelength λ_M) and its superharmonics (wavelengths $\lambda_M/2$, $\lambda_M/3$, etc). However, modes with wavelengths longer than λ_M (defined as subharmonic modes) may also be present and influence the behavior of the ridges. We

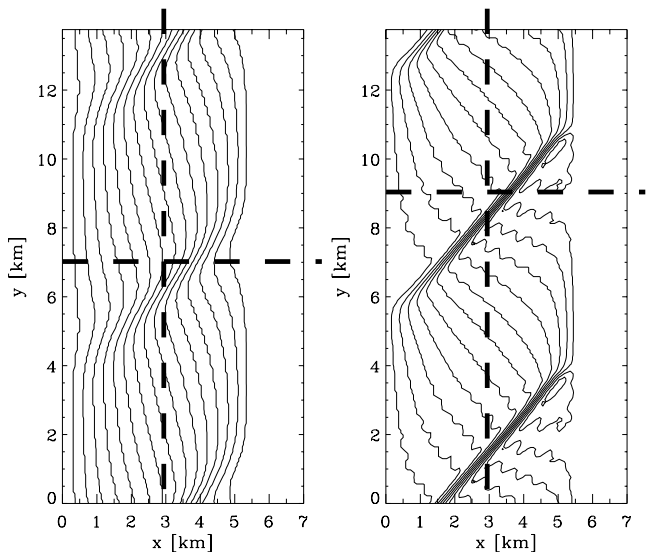

Figure 9. Total depth for $\beta = 2.5 \times 10^{-4}$ (left) at $t = 2400$ yr and (right) at $t = 4800$ yr. Other parameter values representative for the Long Island inner shelf.

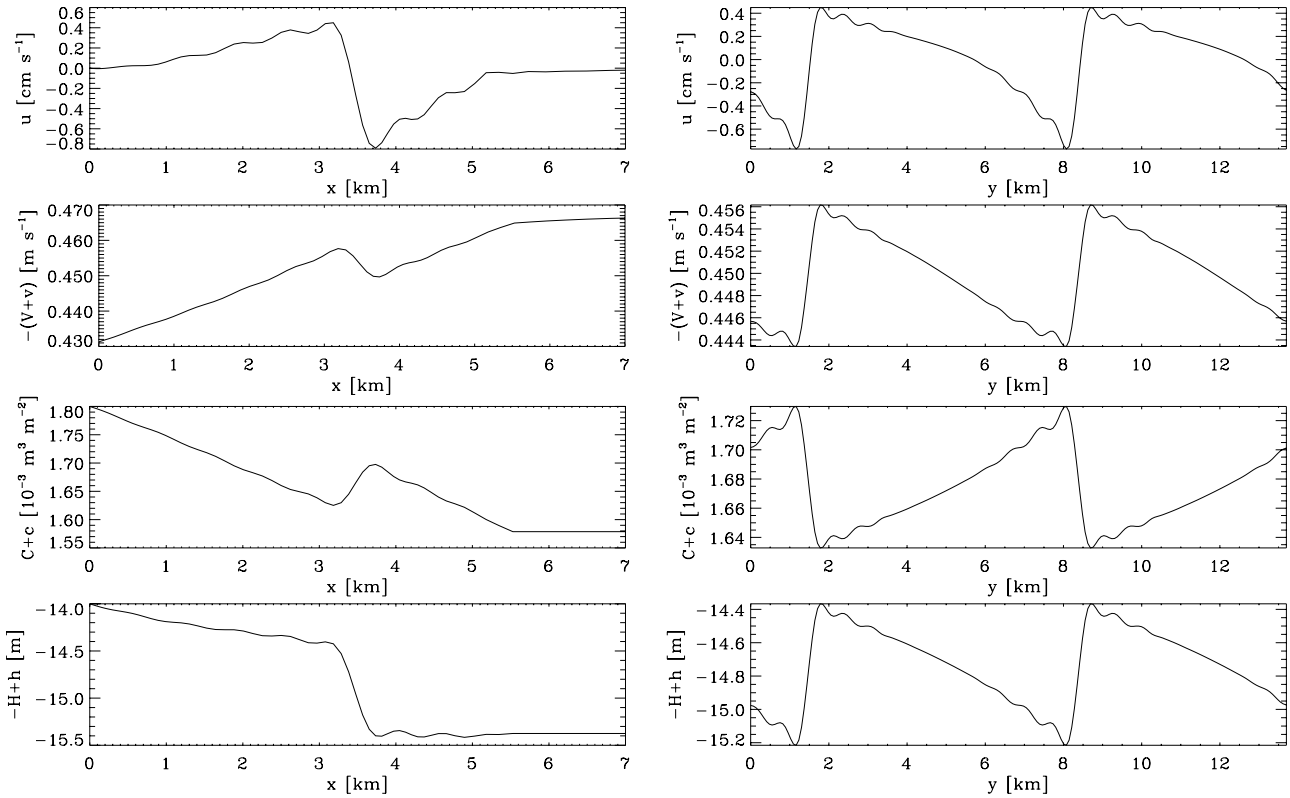

Figure 10. (left) Cross-shelf profiles at y = 9.0 km and (right) along-shelf profiles at x = 3.0 km of velocity components u and $V + v$, total concentration $C + c$, and bottom level $-H + h$ (from top to bottom) at t = 4800 yr for $\beta = 2.5 \times 10^{-4}$.

study this aspect below for a small transverse slope, i.e., $\beta = 1.0 \times 10^{-4}$.

[44] The initially most preferred mode for $\beta = 1.0 \times 10^{-4}$ has an along-shelf wavelength λ_M = 9 km and an e-folding timescale τ = 2000 yr. Computations without subharmonic modes show that only a few modes (J = 8 and N_J = 10) are needed to describe the solution. Nonlinear saturation occurs after ~15000 yr and the bottom perturbation resembles an oblique ridge with the periodicity of 9 km, see Figure 7. By including ($N - 1$) subharmonic modes, the length of the domain in the y direction becomes $L_y = N \times \lambda_M$. The initially most preferred mode is then the (N, 1) mode. To keep the same resolution in the experiments, the number of resolved Fourier modes was taken to be $N \times J$.

[45] In Figure 14 results are shown for N = 8, which is a characteristic value of the ratio between the horizontal extent of a patch of ridges and the wavelength of an individual ridge. The upper left plot shows the time evolution of the different modal amplitudes. The evolution of the maximum and minimum elevation, as well as the total height, of the bottom perturbation is shown in the upper right subplot. Similar results are found for other numbers of subharmonics; experiments were performed up to N = 15. All these experiments show that there is still saturation behavior; that is, the amplitudes become steady in the nontransient stage. Furthermore, the pattern of the perturbation is qualitatively similar to that found for N = 1 (no subharmonics). One effect of adding subharmonic modes is that they cause the saturation time of the individual modes to become considerably longer, so that for instance, when N = 8 it becomes 50000 yr, and hence a factor 3 longer than that obtained for N = 1. On the other hand, the height of the ridges saturates faster if subharmonics are included (see upper right subplot of Figure 14). During the first stage (up to 20000 yr) bottom perturbations resemble shore face–connected ridges with an amplitude and an along-shelf spacing similar to the ones at the final state for N = 1. During the transient state, between 20000 yr and 50000 yr, both the amplitude and the along-shelf spacing of the ridges increase. The values of the individual modes still undergo major changes until 50000 yr. The final height is approximately 0.5 m, i.e., 70% larger than the saturation height obtained for N = 1.

[46] In the saturated state the (5, 1) mode has the largest amplitude (see the Figure 14c). Hence the mode that initially has the largest growth rate is not the dominant mode in the saturated state; in fact it yields no significant contribution to the final perturbation. The shape of the bed forms is almost the same as without subharmonics but with larger wavelength; in this case ~14 km.

[47] Subharmonic modes strongly influence the transient behavior of the perturbations. This can be seen in Figure 14d, which shows the time evolution of the amplitudes of the 5 modes that are dominant at t = 20000 yr. During the first 15000 years the evolution is dominated by linear growth, with the (8, 1) mode having the largest amplitude. After that nonlinear interactions become effective and they cause the excitation of subharmonic modes

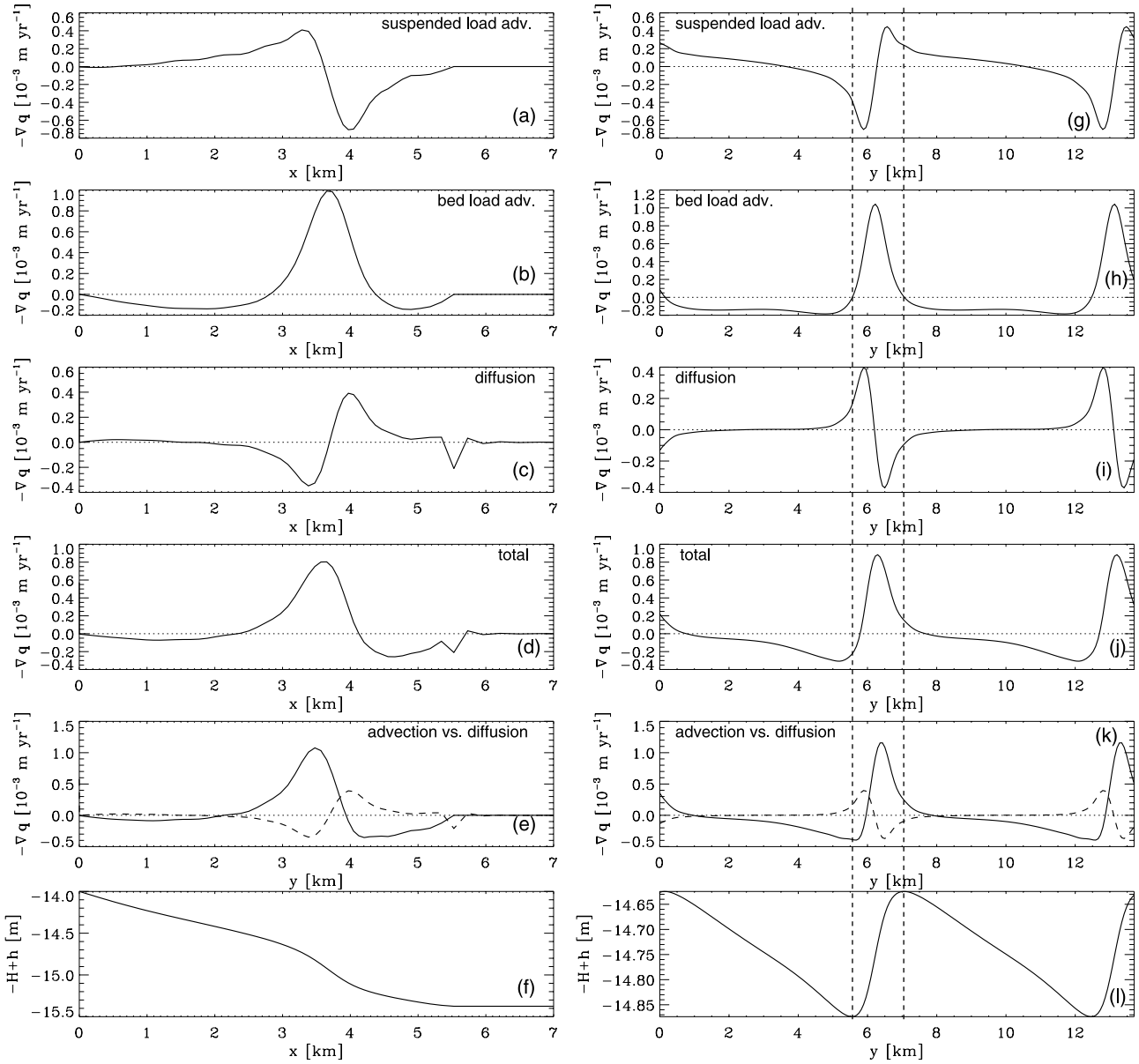

Figure 11. (left) Cross-shelf profiles at y = 7.0 km and (right) along-shelf profiles at x = 3.0 km of different contributions to the divergence of the sediment flux at t = 2400 yr for $\beta = 2.5 \times 10^{-4}$.

and a considerable decay of the initially most preferred mode.

5. Discussion and Conclusions

[48] In this paper a model has been used to investigate the long-term, finite amplitude behavior of shore face–connected sand ridges on storm-dominated microtidal inner shelves. The model is based on concepts introduced by [*Trowbridge*, 1995] and further developed by [*Calvete et al.*, 2001a, 2001b]. In the present study the nonlinear behavior of the perturbations evolving on the basic state has been analyzed by expanding physical variables in eigenmodes of the linearized system. Application of a Galerkin method then yields equations that describe the time evolution of the modal amplitudes. The specific objectives of this paper were threefold. The first was to analyze the physical processes that cause the saturation behavior of the perturbations; that is, after a transient stage their heights become constant. The second was to investigate the effects of adding an along-shelf pressure gradient and taking account of finite settling times of suspended sediment particles in the morphodynamic model on the finite amplitude behavior of the ridges. The last objective was to study the influence of adding new modes in the spectral expansions. The latter include the k = 0 mode (generated by self-interactions of wave-like perturbations) and subharmonic modes (which occur if the along-shelf length of the domain is a multiple of the wavelength of the linearly most preferred mode.

[49] The model was analyzed for values of the parameters that are representative for the inner shelf of Long Island. Results indicate that the model describes the tendency to form migrating shore face–connected sand ridges with

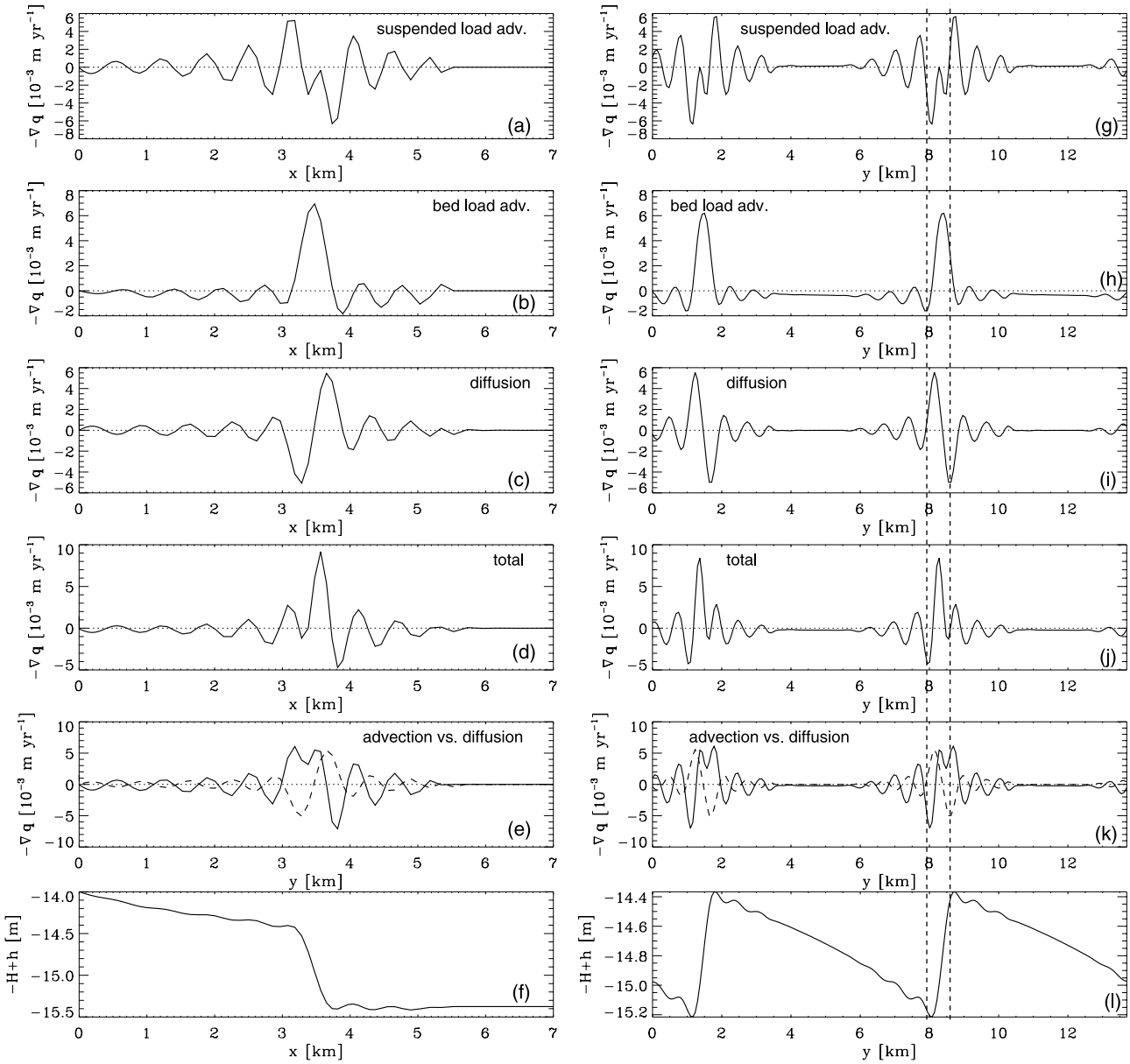

Figure 12. As Figure 11, but at t = 4800 yr and (left) at y = 9.0 km and (right) at x = 3.0 km.

constant amplitudes. Full runs could be carried out for values of the transverse slope up to $\beta = 5.0 \times 10^{-4}$, which is 50% of the measured slope of Long Island inner shelf. For higher values of β runs are still partly successful. The behavior of the solutions is similar to that found in case of smaller values of β, but some time before the saturation stage is reached the solution becomes unbounded. The ridges start to form if $\beta \geq \beta_c \sim 0.5 \times 10^{-4}$ and their final height increases almost linearly up to ~1.8 m for $\beta = 5.0 \times 10^{-4}$. Furthermore, the saturation timescale decreases with increasing β; for $\beta = 5.0 \times 10^{-4}$ a value of 2000 yr is found.

[50] A physical analysis of the model output has shown that saturation is caused by two effects. First, small-scale bed forms are generated by nonlinear processes. These bed forms modify the advective part of the suspended load flux, thereby causing a reduction of the growth of the ridges. Second, the transport of sediment induced by bed slopes

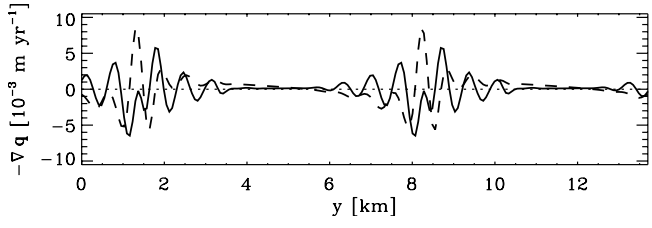

Figure 13. Convergence of the advective part of the suspended load flux at x = 3.0 km as a function of the alongshelf coordinate y at t = 4800 yr. The solid line represents the full quantity (see also Figure 12g), the dashed line shows the contribution, which is linear in the bottom perturbation. The corresponding bottom perturbation is shown in Figure 12l.

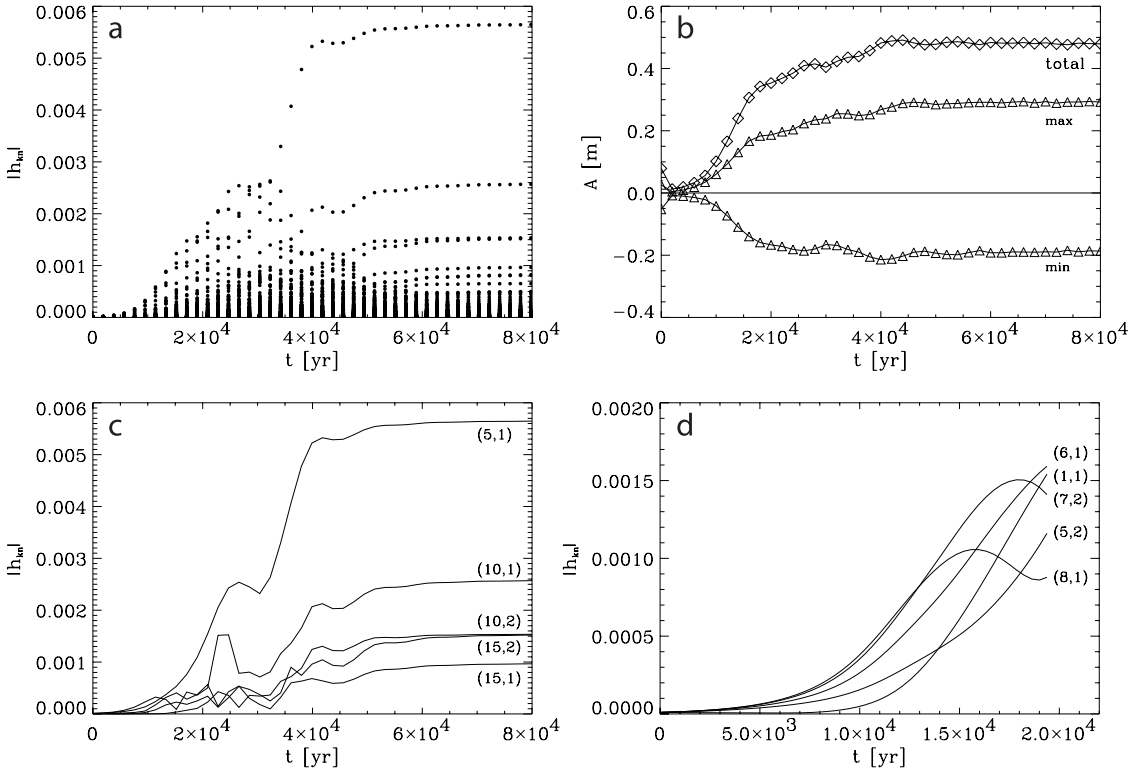

Figure 14. (a) Time evolution of the modal amplitudes in case of $N = 8$ (i.e., seven subharmonic modes) and $\beta = 1.0 \times 10^{-4}$. (b) As Figure 14a but of the maximum and minimum elevation, as well as of the total height, of the bottom perturbation. (c) Time evolution of the amplitudes of the five modes that are the dominant modes in the nontransient stage. (d) As Figure 14c but for the five modes that are dominant at $t = 20000$ yr. For realistic β values the timescales are a factor of 15 smaller.

increases during the evolution of the ridges, because the bottom slopes become steeper.

[51] Sensitivity experiments revealed that adding a longshore pressure gradient, which affects the cross-shelf profile of the storm-driven flow, and a finite settling time of suspended load particles, have only a minor effect on the dynamics. Also the incorporation of the $k = 0$ mode (alongshelf uniform structure) has little effect on the results.

[52] Subharmonic modes significantly affect the dynamics of the ridges. Saturation behavior is still obtained, the shape of the bed forms is almost the same as without subharmonics but with a larger wavelength. The initially most preferred mode is not the dominant mode in the saturated state. The presence of subharmonic modes results in longer saturation times of individual modes, while the height of the ridges saturates on a shorter timescale (compared to that of the modes). In this case, full runs could be performed for transverse slopes up to $\beta = 1.0 \times 10^{-4}$.

[53] We now compare the model results with the field data available for Long Island inner shelf. The obtained dependencies of the final height of the ridges and saturation timescale on the transverse slope (no subharmonics included) allow for an extrapolation to the measured slope. In that case the final height is ~3.5 m, which compares well with the observed height of ~4 m. The corresponding saturation time is ~1000 yr, which is consistent with the lifetime of the ridges. The saturation time is a factor of 15 smaller than that for a slope $\beta = 1.0 \times 10^{-4}$. This information can be used to estimate the saturation time of the ridges in the case that subharmonic modes are included and a measured value of the slope is taken. The result is then ~1300 yr for the saturation time and the final height will be ~5 m.

[54] The present model is subject to various limitations. One problem is that, in case of using a measured value of the transverse slope, solutions become unbounded before the saturation stage is reached. It has been shown that the range of values of the slope for which the model was successful was sufficient to extrapolate the results to higher values of β, thereby allowing for a comparison with field data. Second, the analysis of the saturation process has revealed the importance of small-scale bed forms. It is plausible that these small-scale features can also form as inherent free morphodynamic instabilities, as shown for quasi-steady flow by *Richards* [1980] [see also *Hulscher et al.*, 1993]. In this process secondary circulation in the vertical plane is important. This suggests the use of a three-dimensional model and this is considered as a key topic for future studies. Support for this also comes from field data analyzed by [*Niedoroda et al.*, 1984], which show a clear circulation in the vertical plane perpendicular to the coast. Finally, the effect of sea level changes (~2 m during the last 2000 yr) may be important, considering the timescales on which the ridges evolve. Therefore the sensitivity of the model results to different (but fixed) values of the sea level was investigated. All other parameter values were assumed to be equal

to their values used to simulate the present conditions at the Long Island shelf. Two different values of the transverse bottom slope were investigated: $\beta = 2.5 \times 10^{-4}$ and $\beta = 4 \times 10^{-4}$. The water depth H_0 was decreased from its present 14.4 m to 12.0 m. The results show a weak increase of the height of the ridges and a weak decrease of the saturation time of the height. For example, in case that $\beta = 4 \times 10^{-4}$, the height (saturation time) was 1.31 m (4000 yr) for H_0 = 14.4 m and it was 1.55 m (3000 yr) for H_0 = 12 m. Since the solutions of all these runs showed similar behavior and mutual differences are rather small, we conclude that the model is not very sensitive to changes in sea level within the range of values that we have investigated.

Appendix A: Nonlinear Equations

[55] In the appendices subscripts x, y and t denote differentiation with respect to that variable.

[56] Cross-shelf momentum equation,

$$u\partial_x u + (V+v)\partial_y u - fv = -\partial_x \eta - \frac{\hat{r}_{*0}}{(H-h_0)^{\frac{m}{2}}}\frac{u}{H-h}\,;$$

along-shelf momentum equation,

$$u\partial_x(V+v) + (V+v)\partial_y v + fu =$$
$$-\partial_y \eta - \frac{\hat{r}_{*0}}{(H-h_0)^{\frac{m}{2}}}\frac{V+v}{H-h} + \frac{\hat{r}_{*0}}{H^{\frac{m}{2}}}\frac{V}{H-h}\,;$$

mass equation,

$$\partial_x((H-h)u) + \partial_y((H-h)(V+v)) = 0\,;$$

concentration equation,

$$\partial_x((C+c)u) + \partial_y((C+c)(V+v)) =$$
$$\cdot\, w_s\left(\frac{\hat{c}_{a0}}{(H-h_0)^{\frac{3m}{2}}} - \frac{C+c}{\delta_0 H}\left(1+\frac{h}{H}\right)\right);$$

and sediment equation,

$$\partial_t h + \vec{\nabla}\cdot\vec{q}_b + \vec{\nabla}\cdot\vec{q}_s = 0\,,$$

where

$$\vec{\nabla}\cdot\vec{q}_b = \frac{\nu_b \hat{u}_{w0}^2}{(H-h_0)^m}\left(-m\,\frac{\partial_x(H-h_0)}{H-h_0}\,u + \partial_x u + \partial_x v\right)$$
$$\cdot\,\frac{\nu_b \hat{\lambda}_b}{(H-h_0)^{\frac{3m}{2}}}\left((-3m/2)\,\frac{\partial_x(H-h_0)}{H-h_0}\,\partial_x h + \vec{\nabla}^2 h\right)$$

and

$$\vec{\nabla}\cdot\vec{q}_s = \partial_x((C+c)u) + \partial_y((C+c)(V+v))$$
$$-\frac{\hat{\lambda}_s}{(H-h_0)^{\frac{5m}{2}}}\left((-5m/2)\,\frac{\partial_x(H-h_0)}{H-h_0}\,\partial_x h + \vec{\nabla}^2 h\right)$$

The coefficients in the equations listed above are

$$\hat{r}_{*0} = r_{*0}\,H_0^{\frac{m}{2}}\,, \qquad \hat{u}_{w0} = u_{w0}\,H_0^{\frac{m}{2}}\,,$$

and

$$\hat{c}_{a0} = \left(\frac{\hat{u}_{w0}}{\hat{u}}\right)^3, \qquad \hat{\lambda}_{b0} = \lambda_b \hat{u}_{w0}^3\,, \qquad \hat{\lambda}_{s0} = \lambda_s \hat{u}_{w0}^5\,.$$

Appendix B: Equations for Mode $k = 0$

[57] Cross-shelf momentum equation,

$$u_0\partial_x u_0 + \langle u'\partial_x u'\rangle + \langle v'\partial_y u'\rangle - fv_0 = -\partial_x \eta_0 - \frac{\hat{r}_{*0}}{(H-h_0)^{\frac{m}{2}}}\left\langle\frac{u}{H-h}\right\rangle;$$

along-shelf momentum equation,

$$u_0\partial_x(V+v_0) + \langle u'\partial_x v'\rangle + \langle v'\partial_y v'\rangle + fu_0 =$$
$$-\partial_y \eta_0 - \hat{r}_{*0}(H-h_0)^{\frac{m}{2}}\left\langle\frac{V+v}{H-h}\right\rangle + \frac{\hat{r}_{*0}}{H^{\frac{m}{2}}}\left\langle\frac{V}{H-h}\right\rangle;$$

mass equation,

$$\partial_x((H-h_0)u_0) - \partial_x\langle h'u'\rangle = 0\,;$$

concentration equation,

$$\partial_x((C+c_0)u_0) + \partial_x\langle c'u'\rangle =$$
$$\cdot\, w_s\left(\frac{\hat{c}_{a0}}{(H-h_0)^{\frac{3m}{2}}} - \frac{C+c_0}{\delta_0 H}\left(1+\frac{h_0}{H}\right) - \frac{\langle c'h'\rangle}{\delta_0 H^2}\right);$$

and sediment equation,

$$\partial_t h_0 + \left\langle\vec{\nabla}\cdot\vec{q}_b\right\rangle + \left\langle\vec{\nabla}\cdot\vec{q}_s\right\rangle = 0\,,$$

where

$$\left\langle\vec{\nabla}\cdot\vec{q}_b\right\rangle = \frac{\nu_b \hat{u}_{w0}^2}{(H-h_0)^m}\left(-m\,\frac{\partial_x(H-h_0)}{H-h_0}\,u_0 + \partial_x u_0\right)$$
$$-\frac{\nu_b \hat{\lambda}_b}{(H-h_0)^{\frac{3m}{2}}}\left((-3m/2)\,\frac{\partial_x(H-h_0)}{H-h_0}\,\partial_x h_0 + \partial_{xx}^2 h_0\right)$$

and

$$\left\langle\vec{\nabla}\cdot\vec{q}_s\right\rangle = \partial_x((C+c_0)u_0) + \partial_x\langle c'u'\rangle$$
$$-\frac{\hat{\lambda}_s}{(H-h_0)^{\frac{5m}{2}}}\left((-5m/2)\,\frac{\partial_x(H-h_0)}{H-h_0}\,\partial_x h_0 + \partial_{xx}^2 h_0\right)$$

[58] **Acknowledgments.** This work has been jointly funded by the National Institute of Coastal and Marine Management/RIKZ, Netherlands, and the EU-sponsored HUMOR project (contract EVK3-CT-2000-00037).

References

Antia, E. E., Shoreface–connected ridges in German and US mid-Atlantic bights: Similarities and contrasts, *J. Coastal Res.*, *12*, 141–146, 1996.

Bailard, J. A., An energetics total load sediment transport model for a plane sloping beach, *J. Geophys. Res.*, *86*, 10,938–10,954, 1981.

Calvete, D., A. Falqués, H. E. de Swart, and N. Dodd, Nonlinear modelling of shoreface–connected sand ridges, in *Proceedings of Coastal Sediments 1999*, vol. 2, edited by N. C. Kraus and W. G. McDougal, pp. 1123–1138, Am. Soc. of Civ. Eng., Reston, Va., 1999.

Calvete, D., A. Falqués, H. E. de Swart, and M. Walgreen, Modelling the formation of shoreface–connected sand ridges on storm-dominated shelves, *J. Fluid. Mech.*, *441*, 169–193, 2001a.

Calvete, D., M. Walgreen, H. E. de Swart, and A. Falqués, A model for sand ridges on the shelf: Effect of tidal and steady currents, *J. Geophys. Res.*, *106*, 9311–9326, 2001b.

Calvete, D., H. E. de Swart, and A. Falqués, Effect of depth-dependent stirring on the final amplitude of shoreface–connected sand ridges, *Cont. Shelf Res.*, *22*, 2763–2776, 2002.

Canuto, C., M. Y. Hussaini, A. Quarteroni, and T. A. Zang, *Spectral Methods in Fluid Dynamics*, Springer-Verlag, New York, 1988.

Duane, D. B., M. E. Field, E. P. Miesberger, D. J. P. Swift, and S. Williams, Linear shoals on the Atlantic continental shelf, Florida to Long Island, in *Shelf Sediment Transport: Process and Patterns*, edited by D. J. P. Swift, D. B. Duane, and O. H. Pilkey, Van Nostrand Reinhold, New York, 1972.

Falqués, A., D. Calvete, H. E. de Swart, and N. Dodd, Morphodynamics of shoreface–connected ridges, in *Coastal Engineering 1998*, edited by B. L. Edge, pp. 2851–2864, Am. Soc. of Civ. Eng., Reston, Va., 1998a.

Falqués, A., D. Calvete, and A. Montoto, Bed-flow instabilities of coastal currents, in *Physics of Estuaries and Coastal Seas*, edited by J. Dronkers and M. B. A. M. Scheffers, pp. 417–424, Balkema, Rotterdam, 1998b.

Hulscher, S. J. M. H., H. E. de Swart, and H. J. de Vriend, The generation of offshore tidal sand banks and sand waves, *Cont. Shelf Res.*, *13*, 1183–1204, 1993.

Karniadakis, G. E., M. Israeli, and S. A. Orszag, high-order splitting methods for the incompressible Navier-Stokes equations, *J. Comput. Phys.*, *97*, 414–443, 1991.

Komarova, N. L., and A. C. Newell, Nonlinear dynamics of sand banks and sand waves, *J. Fluid. Mech.*, *415*, 285–321, 2000.

Niedoroda, A. W., and D. J. P. Swift, Maintenance of the shoreface by wave orbital currents and mean flow: Observations from the Long Island coast, *Geophys. Res. Lett.*, *8*, 337–340, 1981.

Niedoroda, A. W., D. J. P. Swift, T. S. Hopkins, and C. H. Ma, Shoreface morphodynamics on wave-dominated coasts, *Mar. Geol.*, *60*, 331–354, 1984.

Parker, G., N. W. Lanfredi, and D. J. P. Swift, Seafloor response to flow in a Southern Hemisphere sand-ridge field: Argentina inner shelf, *Sediment. Geol.*, *33*, 195–216, 1982.

Richards, K. J., The formation of ripples and dunes on an erodible bed, *J. Fluid Mech.*, *99*, 597–618, 1980.

Scott, J. T., and G. T. Csanady, Nearshore currents off Long Island, *J. Geophys. Res.*, *81*, 5401–5409, 1976.

Swift, D. J. P., and M. E. Field, Evolution of a classic sand ridge field: Maryland sector, North American inner shelf, *Sedimentology*, *28*, 461–482, 1981.

Swift, D. J. P., G. Parker, N. W. Lanfredi, and G. P. K. Figge, Shoreface–connected sand ridges on American and European shelves: A comparison, *Estuarine Coastal Mar. Sci.*, *7*, 257–273, 1978.

Swift, D. J. P., A. W. Niedoroda, C. E. Vincent, and T. S. Hopkins, Barrier island evolution, Middle Atlantic Shelf, U.S.A., part 1: Shoreface dynamics, *Mar. Geol.*, *63*, 331–361, 1985.

Trowbridge, J. H., A mechanism for the formation and maintenance of shore-oblique sand ridges on storm-dominated shelves, *J. Geophys. Res.*, *100*, 16,071–16,086, 1995.

van de Meene, J. W. H., and L. C. van Rijn, The shoreface–connected ridges along the central Dutch coast—part 1: Field observations, *Cont. Shelf Res.*, *20*, 2295–2323, 2000.

van Rijn, L. C., *Principles of Sediment Transport in Rivers, Estuaries and Coastal Seas*, Aqua, Amsterdam, 1993.

D. Calvete, Department Física Aplicada, Universitat Politècnica de Catalunya, Campus Nord - Mòdul B4, Jordi Girona 1-3, 08034 Barcelona, Spain. (calvete@fa.upc.es)

H. E. de Swart, Institute for Marine and Atmospheric Research, Utrecht University, Princetonplein 5, 3584 CC Utrecht, Netherlands. (h.e.deswart@phys.uu.nl)